

Vector modulation instability induced by vacuum fluctuations in highly birefringent fibers in the anomalous dispersion regime

D. Amans, E. Brainis, M. Haelterman, and Ph. Emplit

*Optique et acoustique, Université Libre de Bruxelles,
avenue F.D. Roosevelt 50, CP 194/5, 1050 Bruxelles, Belgium*

S. Massar

*Laboratoire d'information quantique and QUIC,
Université Libre de Bruxelles, avenue F.D. Roosevelt 50,
CP 165/59, 1050 Bruxelles, Belgium*

We report a detailed experimental study of vector modulation instability in highly birefringent optical fibers in the anomalous dispersion regime. We prove that the observed instability is mainly induced by vacuum fluctuations. The detuning of the spectral peaks agrees with linear perturbation analysis. The exact shape of the spectrum is well reproduced by numerical integration of stochastic nonlinear Schrödinger equations describing quantum propagation.

© 2018 Optical Society of America

OCIS codes: 000.1600, 060.4370, 190.3270, 190.4380.

In birefringent silica fibers, stable propagation of a monochromatic wave can be inhibited by a nonlinear process called *vector* modulation instability (V-MI) in both dispersion regimes (normal or anomalous).^{1,2,3} This contrasts with the *scalar* modulation instability (S-MI) that does not require birefringence but can only arise in the anomalous dispersion regime (at least when second order dispersion dominates^{4,5}). Two limits, those of weak and strong birefringence, are amenable to relatively simple analytical study.⁶ These predictions have been confirmed experimentally in a number of cases,^{7,8,9} particularly in the normal dispersion regime.

The only experimental investigation of V-MI in the anomalous dispersion regime that we are aware of is a recent unsuccessful attempt using photonic crystal fibers.¹⁰ Here we report what is to our knowledge the first experimental study of V-MI in strongly birefringent silica fibers in the anomalous dispersion regime. We also carry out a very precise comparison between experimental results and the predictions of numerical simulations.

Modulation instabilities (MI) can be induced by classical noise present initially together with the pump beam. But MI can also arise spontaneously through amplification of vacuum fluctuations.¹¹ In practice classical input noise and vacuum fluctuations compete for inducing MI. The experiment reported here is carried out in the regime where the quantum noise is dominant.

Elsewhere,¹² we present an unified approach to the problem of scalar and vector MI based on the *stochastic nonlinear Schrödinger equations* (SNLSE) which generalizes the work of Ref. 13. This approach is particularly well suited for numerical simulations in complex situations where classical noise and vacuum fluctuations act together, where the pump is depleted, or where the higher order harmonics of MI appear. In previous work on modulation instability, comparison between theory and experiment has generally been limited to noting that the frequency at which the maximum gain of the MI occurs is correctly predicted. Here we show that there is excellent agreement between the experimental results and the numerical integration of the SNLSE. In particular the detailed shape of the output spectrum can be predicted in detail, even in the case where higher order harmonics appear (which cannot be predicted by linear perturbation theory). To our knowledge this is the first time experimental and theoretical studies of MI are compared in such detail. A related work is the comparison between theory and experiment for RF noise measurements reported in Ref. 14.

The experimental setup is reported in Fig. 1. It consists of a Q switched laser (Cobolt Tango) that produces pulses at 1536 nm, with a 3.55 ns full-width-at-half-maximum (FWHM) duration τ and a 2.5 kHz repetition rate f . The Gaussian spectral shape of the laser has been characterized using a Fabry-Perot interferometer. The measured 0.214 GHz FWHM spectral width is slightly larger than expected in the Fourier transform limit. The pump power is adjusted using variable neutral density filters (ND). We measured the injected mean power P_m at the end of the fiber. The peak power P_0 is related to the mean power according to the relation:

$$P_0 = 2\sqrt{\frac{\ln(2)}{\pi}} \frac{P_m}{f\tau} = 1.06 \times 10^5 P_m, \quad (1)$$

A polarizing beam splitter (PBS1) ensures the pump pulse is linearly polarized. A half-wave plate is used to tune the angle θ between the pump polarization direction and the principal axes of the fiber. A polarizing beam splitter (PBS2) can be used in order to observe the field components polarized along the fast or slow axes separately. Lastly, spectra are recorded using an optical spectral analyser (OSA). In our experiment we use the Fibercore HB1250P optical fiber. The fiber length $L = 51$ m, the group-velocity dispersion (GVD) parameter $\beta_2 = -15 \text{ ps}^2 \text{ km}^{-1}$ and the group-velocity mismatch parameter $\Delta\beta_1 = 286.1 \text{ fs m}^{-1}$ have been measured by independent methods (only significant digits have been indicated). Note that the accuracy on the value of β_2 is poor compared to the standards. This is because the interferometric method¹⁵ that we used turned out to be difficult to implement with a birefringent fiber. The group-velocity mismatch parameter $\Delta\beta_1$ is deduced from the walk-off between pulses propagating on the principal axes of the fiber. The fiber length L is deduced from a measurement of the pulse time of flight. The other important parameters of the fiber, and a more accurate estimation of β_2 , can be inferred from MI spectral peaks positions, as explained further.

Fig. 2 shows a typical spectrum at the fiber output when the angle θ is set to 45 degrees. The fast and slow polarization components have been separated using PBS2 and their spectra recorded successively. The plot clearly exhibits two V-MI peaks at 1511.4 nm and 1561.4 nm that are polarized along the fast and slow axes respectively. It also shows S-MI peaks at 1530.0 nm and 1541.9 nm, with first harmonics. In contrast with V-MI, S-MI is equally generated on both principal axes. By polarizing the input field along the fast or slow axes, we have observed that V-MI disappears and that the amplitude of the S-MI peaks increases

dramatically (figure not shown).

According to linear perturbation analysis, the angular frequency shifts from the pump of the MI peaks are given by

$$\Delta\Omega_{S-MI}^2 \approx \frac{\gamma P_0}{|\beta_2|} \left[1 - \frac{2\gamma P_0}{9|\beta_2|} \left(\frac{|\beta_2|}{\Delta\beta_1} \right)^2 \right] \quad (2)$$

$$\Delta\Omega_{V-MI}^2 \approx \left(\frac{\Delta\beta_1}{|\beta_2|} \right)^2 \left[1 + \frac{2\gamma P_0}{|\beta_2|} \left(\frac{|\beta_2|}{\Delta\beta_1} \right)^2 \right] \quad (3)$$

for S-MI and V-MI peaks respectively. Here, γ stands for the Kerr nonlinearity parameter of the fiber. Fig. 3 shows the evolution of the spectrum of light emerging from the fiber when the pump power is increased. Using Eqs. (2) and (3), the ratios $\frac{\Delta\beta_1}{|\beta_2|} = 18.740$ (rad) THz and $\frac{\gamma}{|\beta_2|} = 0.2135$ (rad) THz² W⁻¹ were deduced from these measurements. The first ratio and the measured value of $\Delta\beta_1$ permits to infer that $\beta_2 = -15.27$ ps² km⁻¹, which is compatible with the independently measured value. From the second ratio, we deduce that $\gamma = 3.26$ W⁻¹ km⁻¹.

The exponential growth of the MI peaks and harmonics is clearly apparent on Fig. 3. From these measurements we deduce that the ratio between the maximum gain of the V-MI and of the S-MI is 0.67 ± 0.05 , in good agreement with the theoretical value $2/3$. We also find that the ratio between the maximum gain of the 1st harmonic and of the S-MI is 1.88 ± 0.15 , in good agreement with the theoretical value^{16,17} of 2.

We now focus on the quantitative comparison between experimental spectral amplitudes and those predicted by the SNLSE model for spontaneous (or vacuum-fluctuations induced) modulation instabilities. This comparison makes sense because the exact shape of the spectrum, and in particular the relative intensities of the modulation instability peaks and harmonics, is very strongly dependent on the initial noise and pump peak power. Experimental and computed spectra are plotted together in Fig. 4. In the simulations we used the parameters deduced from experimental MI peaks positions (see above), but in order to obtain a good fit we had to increase the peak pump power by 5% with respect to that deduced from the measurements using Eq. (1). We are not sure of the origin of this discrepancy. It could either be due to a systematic error in the measured values of P_m , to an error in the experimental measure of $\Delta\beta_1$, to the fact that the experimental pulses are not exactly Fourier-transform limited, or to some classical noise photons (for instance due to Raman scattering in the fiber) that are added to vacuum fluctuations and slightly speed up the

instability. In any case the discrepancy is small enough to confidently conclude that in our experiment the MI is mainly induced by vacuum-fluctuations. Indeed with this small adjustment the experimental MI spectra are very well reproduced by numerical integration of the SNLSE model.

In summary, we report what is to our knowledge the first experimental observation of spontaneous vector modulation instability in a highly birefringent silica fiber in the anomalous dispersion regime. The pump power dependence of the detuning of both scalar and vector side-bands, as well as their polarizations, agree with linear perturbation theory when the pump depletion is small. We have also obtained very good agreement between the experimental spectra and those obtained by numerical integration of the SNLSE derived from the quantum theory. This is to our knowledge the first time that theoretical and experimental spectra are compared in such quantitative detail. This very good agreement between the two approaches proves that the modulation instability that we observed was truly spontaneous, in the sense that it mainly results from the amplification of vacuum-fluctuations.

Acknowledgments

This research is supported by the Interuniversity Attraction Poles Programme - Belgium Science Policy - under grant V-18. We are also grateful to Fonds Defay for financial support.

References

1. A. Hasegawa, Phys. Lett. **53A**, 103 (1975).
2. S. Trillo, S. Wabnitz, J. Opt. Soc. Am. B **9**, 1061 (1992).
3. J. Hong, W. P. Huang, IEEE J. Quantum Electron. **28**, 1838 (1992).
4. S. Pitois, G. Millot, Opt. Commun. **226**, 415 (2003).
5. J. D. Harvey, R. Leonhardt, S. Coen, R. Leonhardt, G. K. L. Wong, J. C. Knight, W. J. Wadsworth, Ph. St. J. Russell, Opt. Lett. **28**, 2225 (2003).
6. G. P. Agrawal, *Nonlinear Fiber Optics, third ed.* (Academic Press, San Diego, 2001).
7. J. E. Rothenberg, Phys. Rev. A **42**, 682 (1990).
8. P. D. Drummond, T. A. B. Kennedy, J. M. Dudley, R. Leonhardt, J. D. Harvey, Opt. Commun. **78**, 137 (1990).
9. S. G. Murdoch, R. Leonhardt, J. D. Harvey, Opt. Lett. **20**, 866 (1995).
10. B. Kibler, C. Billet, J. M. Dudley, R. S. Windeler, G. Millot, Opt. Lett. **29**, 1903 (2004).

11. M. J. Potasek and B. Yurke, *Phys. Rev. A* **35**, 3974 (1987).
12. E. Brainis, D. Amans, and S. Massar, submitted to *Phys. Rev. A*, <http://xxx.lanl.gov/abs/quant-ph/0412096>.
13. T. A. B. Kennedy, *Phys. Rev. A* **44**, 2113 (1991).
14. K. L. Corwin, N. R. Newbury, J. M. Dudley, S. Coen, S. A. Diddams, K. Weber, R. S. Windeler, *Phys. Rev. Lett.* **90**, 113904 (2003).
15. P. Merritt, R. P. Tatam, and D. A. Jackson, *J. Lightwave Technol.* **7**, 703 (1989).
16. A. Hasegawa and W. F. Brinkman, *IEEE J. Quantum Electron.* **16**, 694 (1980).
17. K. Tai, A. Hasegawa, and A. Tomita, *Phys. Rev. Lett.* **56**, 135 (1986).

List of Figure Captions

Fig. 1. Experimental setup. ISO: isolator, ND: variable neutral density filter, PBS: polarizing beam splitters, PMF: polarization maintaining fiber, and OSA: optical spectrum analyser.

Fig. 2. Spectra of the fast (black curve) and slow (gray curve) polarization components of the light emerging from the fiber. The light is injected with a polarization angle $\theta = 45^\circ$ relative to the principal axes of the fiber. The mean power is approximately 1 mW. The resolution bandwidth is 1 nm.

Fig. 3. Spectrum of the output field for increasing pump mean power, respectively 1.065 mW, 1.105 mW, 1.145 mW, 1.165 mW, and 1.265 mW. The light is injected with a polarization angle $\theta = 45^\circ$ relative to the principal axes of the fiber. The resolution bandwidth is 0.1 nm.

Fig. 4. Comparison between experimental spectra (black curves) and numerical integration of the SNLSE (grey curves). The numerical results are noisy because only one realization of the stochastic method has been computed for each curve. The flat parts on the experimental spectra correspond to the sensibility limit of the OSA. In the simulations the pump pulse is assumed to be Fourier transform limited. The simulation parameters are $\lambda_0 = 1536$ nm, $\tau = 3.55$ ns, $L = 51$ m, $\gamma = 3.26$ W⁻¹km⁻¹, $\beta_2 = -15.26$ ps²km⁻¹ and $\Delta\beta_1 = 286.1$ fs m⁻¹. The peak powers P_0 corresponding to simulations (experiments) are (a) 132.5 W (125.6 W), (b) 127.2 W (121.4 W), and (c) 116.6 W (112.9 W). The numerical results have been convolved with a response function to take into account the resolution of the OSA.

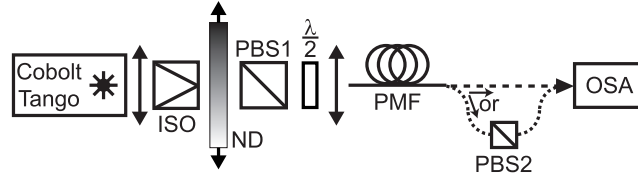


Fig. 1. Experimental setup. ISO: isolator, ND: variable neutral density filter, PBS: polarizing beam splitters, PMF: polarization maintaining fiber, and OSA: optical spectrum analyser. Amans57847F1.eps

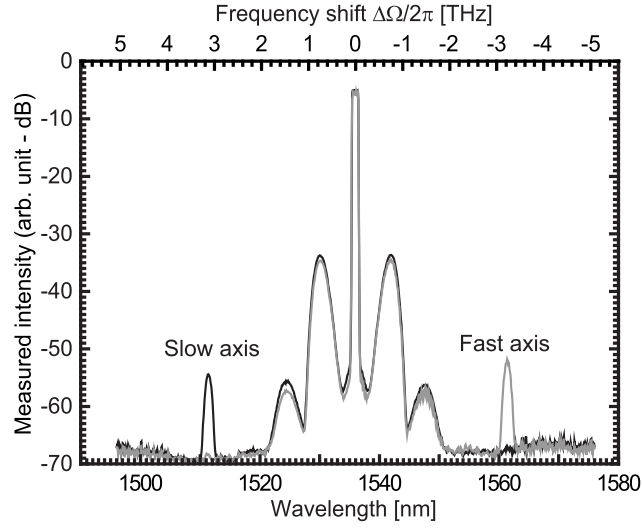


Fig. 2. Spectra of the fast (black curve) and slow (gray curve) polarization components of the light emerging from the fiber. The light is injected with a polarization angle $\theta = 45^\circ$ relative to the principal axes of the fiber. The mean power is approximately 1 mW. The resolution bandwidth is 1 nm. Amans57847F2.eps

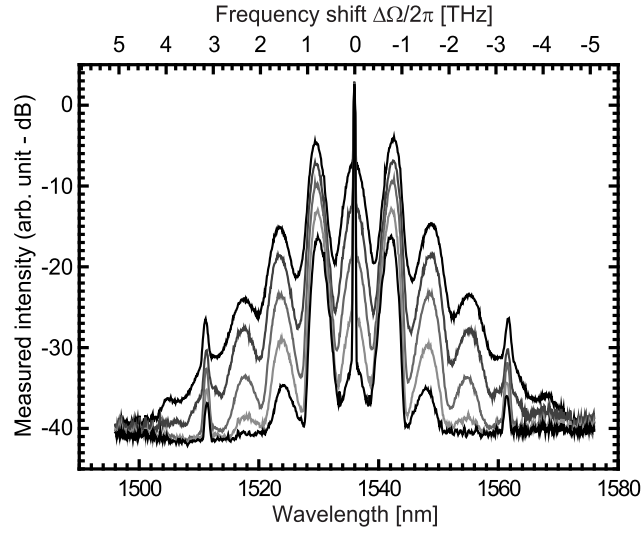


Fig. 3. Spectrum of the output field for increasing pump mean power, respectively 1.065 mW, 1.105 mW, 1.145 mW, 1.165 mW, and 1.265 mW. The light is injected with a polarization angle $\theta = 45^\circ$ relative to the principal axes of the fiber. The resolution bandwidth is 0.1 nm. Amans57847F3.eps

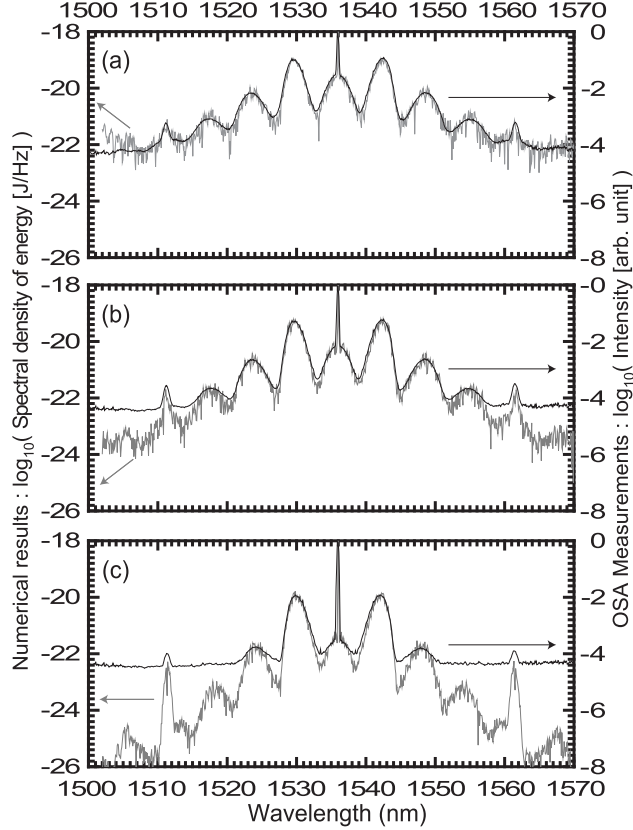


Fig. 4. Comparison between experimental spectra (black curves) and numerical integration of the SNLSE (grey curves). The numerical results are noisy because only one realization of the stochastic method has been computed for each curve. The flat parts on the experimental spectra correspond to the sensibility limit of the OSA. In the simulations the pump pulse is assumed to be Fourier transform limited. The simulation parameters are $\lambda_0 = 1536$ nm, $\tau = 3.55$ ns, $L = 51$ m, $\gamma = 3.26$ W⁻¹km⁻¹, $\beta_2 = -15.26$ ps²km⁻¹ and $\Delta\beta_1 = 286.1$ fs m⁻¹. The peak powers P_0 corresponding to simulations (experiments) are (a) 132.5 W (125.6 W), (b) 127.2 W (121.4 W), and (c) 116.6 W (112.9 W). The numerical results have been convolved with a response function to take into account the resolution of the OSA.

Amans57847F4.eps